

Test results of the ASIC Front-end Trigger Prototypes for the Muon Barrel Detector of CMS at LHC

M. De Giorgi¹, C. Grandi², U. Dosselli¹, F. Gasparini¹, U. Gasparini¹, F. Gonella¹, P. Guaita¹, I. Lippi¹, A. Meneguzzo¹, M. Passaseo¹, M. Pegoraro¹, P. Ronchese¹, A. J. Ponte Sancho^{1,a}, R. Martinelli¹, E. Torassa¹, L. Ventura¹, P. Zotto³, G. Zumerle¹

- 1) *Dip. di Fisica dell'Università di Padova and Sezione I.N.F.N. di Padova, Italy*
 - 2) *CERN, European Organization for Particle Physics, Geneva, Switzerland*
 - 3) *Dip. di Fisica del Politecnico di Milano and Sezione I.N.F.N. di Padova, Italy*
- a) *Now at Universidade do Algarve, UCEH, Gambelas, Faro, Portugal*

(Submitted to Nuclear Instruments and Methods)

Abstract

A sample of ASIC prototypes of the first level trigger front-end device for the muon barrel drift chambers of CMS was tested on a full size chamber prototype.

Tests were performed at several incident angles on cosmic rays and at normal incidence using a muon beam. The chamber was irradiated using a ¹³⁷Cs gamma source to simulate the LHC radiation environment.

The performance of the tested prototypes with respect to efficiency, resolution and noise issues is reported.

1. Introduction

The LHC accelerator imposes severe requirements to the first level muon trigger system of any proposed detector. The trigger time resolution should be much better than the 25 ns time interval between successive pp interactions to assure the parent bunch crossing identification and the momentum resolution should provide the best possible p_T assignment for the trigger candidate to allow fast selection of interesting events.

The easiest way to meet the timing requirement is the selection of a fast response detector, for instance made of Resistive Plate Counters. The CMS [1] experiment has adopted a scheme in which this kind of detector is integrated with a more sophisticated trigger based on the tracking chambers.

The proposed trigger baseline for the barrel detector is designed in order to be able to make a rough local track segment reconstruction and to uniquely identify the parent bunch crossing of the track candidate. The algorithm developed to meet these requirements was implemented in the front-end trigger device, referred to as Bunch and Track Identifier (BTI). Other devices [2,3] are needed in the overall trigger scheme to perform track candidates selection, noise suppression, association of segments of tracks in different chambers and p_T assignment.

2. Experimental Setup

The tests were performed at the CERN Gamma Irradiation Facility (GIF) in August 1998 exposing a full size chamber to a muon beam with energies in the range 80-100 GeV and during winter 1998-1999 in the Legnaro INFN National Laboratories, exposing it to cosmic rays.

The chamber prototype consists of three groups of four layers (called Superlayers) of 47 drift tubes each. The layers are staggered by half a tube in order to solve the left-right ambiguity.

The trigger performance is largely connected to the drift cell design that was optimized for linearity of the space-time relationship by means of two C-shaped cathodes and two shaping electrodes facing the wire as shown in Figure 1. The main problem is the equalization of the drift paths to the anode. This equalization can be assured at low incidence angle, but a linearity degradation is expected when this angle becomes larger, since the time difference between the drift paths increases. In order to limit the variation it is necessary to reduce the active cell zone and therefore the final choice is a trade off between linearity and efficiency.

The results on the performance of the drift cell are presented elsewhere [4].

The wires were readout with an ASIC prototype of the MAD amplifier [5] operated at a threshold of 6fC.

Two Superlayers were equipped with a card carrying eight BTI ASICs. The BTI is a synchronous device and therefore its performance is strictly related to the phase of the clock with respect to the particle crossing time. A 80 MHz FIFO unit [6] was used to identify the 25 ns time slot assigned to the BTI trigger: the BTI computed parameters corresponding to any time slot were stored within the FIFO.

The data were recorded using 960 MHz TDCs with multihit capability [7].

3. Description of the Bunch and Track Identifier

The Bunch and Track Identifier is the implementation of a trigger device based on the generalized mean-timer method [8]. It was explicitly developed to extend the technique to work on groups of four layers of staggered drift tubes, aiming to the identification of the tracks giving signals in at least three out of the four planes.

This method relies on the fact that the particle path is a straight line and the wire positions along the path (the measurement points) are equidistant. Therefore, considering the drift times of any three adjacent planes of staggered tubes (e.g. cells in layers A, B and C of Figure 2), the relation

$$T_{MAX} = \frac{T_A + 2T_B + T_C}{2}$$

where T_{MAX} is the maximum drift time to the wire, holds independently of the track impact point and angle of incidence. Actually the BTI digitizes the time T_s after particle detection at 80 MHz frequency and at every clock count computes the apparent drift time $T = T_{MAX} - T_s$, where T_{MAX} is a programmable parameter depending on drift velocity. This calculation gives the real drift times only at the time T_{MAX} after particle crossing. Therefore the digitized times have values satisfying the relation only at that clock count, while the relation does not hold true at any other time.

This constant time difference, between the particle crossing and the detection of the relation validity, allows the identification of the parent bunch crossing.

In fact it occurs that at the time T_{MAX} the drift times are aligned: i.e. the hits form an image of the muon track, thus allowing the extraction of the full track information (track impact position and direction).

Extending the method to four layers, implies that the bunch crossing identification is possible even if the drift time of a tube is missing, due to inefficiency, or wrong, due to the emission of a δ -ray masking the good hit, since there are still three useful cells giving the minimum requested information. The mean timer method is also insensitive to all uncorrelated single hits and it is therefore well-suited to a high radiation environment.

3.1 Design of the BTI ASIC

Each BTI is connected to nine wires allocated as shown in Figure 2. Each Superlayer is equipped with one BTI every four wires and therefore the BTIs are overlapped by five wires, i.e. the next BTI will start from cell labeled 5 in Figure 2. This overlap assures a high angular acceptance and the redundancy needed to limit the inefficiency in case of a BTI failure.

The evaluated parameters are the position, computed in the Superlayer centre, and the angular k-parameter $k = h \tan \psi$, with ψ being the angle of the track with respect to the normal to the chamber plane in the transverse projection and $h = 13mm$ being the distance between the wire planes.

The actual BTI candidate track finding algorithm computes in parallel several track patterns hypotheses: a pattern is identified by a sequence of wire numbers and labels stating if the track crosses the tube on the right or on the left of the given wire (e.g. in Figure 2 the track corresponds to the pattern 5L3R6L4R). Any given pattern includes six couples of planes (AB, BC, CD, AC, BD, AD), each one providing a measurement of the position (through a *x-equation*) and of the k-parameter (through a *k-equation*) of the track.

The equations are computed at every cycle using the hit arrival time with 12.5ns resolution. The value of a *k-equation* corresponds to a rough measurement of the track direction at that cycle and is time dependent. Therefore each couple included in a pattern gives its own measurement of the track direction: the hits are aligned when, after applying a couple dependent proportional factor, the values of the k-parameter computed for each couple are equal.

Hence at every clock cycle the whole set of *k-equations* is computed and a BTI trigger is generated if at least three of the six k-parameters associated to any of the patterns are in coincidence. The coincidence of the *k-equations* values is verified within a programmable tolerance window. This tolerance is defined according to the resolution of each couple that in turn depends on the distance between the wires and was chosen to allow a maximum cell linearity error equivalent to 25ns. The coincidence allows the bunch crossing identification owing to the time-dependence of the *k-equations* value.

If there is a coincidence of all the six k-parameters, the trigger corresponds to the alignment of four hits and it is marked as High Quality Trigger (HTRG), while in any other case, with a minimum of three coincident k-parameter, it is due to the alignment of only three hits and it is marked Low Quality Trigger (LTRG). The angular resolution is track pattern dependent and is generally worse for LTRGs.

If several track patterns give a response, the HTRG is chosen as the triggering track pattern. If there is more than one HTRG or the triggers are all LTRGs, the first one, in an arbitrarily defined order, is selected.

The request of the alignment of any three hits is a substantial source of background, since it introduces effects creating false triggers. There is a probability that the alignment of four hits at some clock step produces the alignment of only three of them at the step just before or after the HTRG signal, thus generating *ghost* LTRG candidate tracks. There is also some probability that a random LTRG could happen at any clock step with some fancy k-parameter due to the left-right ambiguity, that is duplicating the possible choices for every hit. Finally the δ -rays produced inside the cell will provide wrong time measurement enhancing the probability of an out of time trigger formed using the wrong measurement.

The noise reduction of the former kind of *ghosts* is obtained issuing the LTRG signal only if at the neighbouring steps there is not any HTRG generated: this mechanism is called Low Trigger Suppression (LTS). The noise reduction of the latter kind of *ghosts* is obtained acting on tolerances in the association phase of the following stages of the trigger. These algorithms do not add any latency to the BTI flow.

The impact position of the muon is not entering the track selection algorithm and it is computed only at the end of the process for the selected triggering pattern.

Position and angular resolution depend on the drift velocity and on the sampling frequency of the device. The drift velocity without magnetic field and for the gas mixture used in the prototype (Ar/CO₂-85/15) is 56 μ m/ns and the foreseen sampling frequency is 80MHz. In these conditions the angle is measured with a least count better than 60mrad and the position is measured with a least count of 1.4mm.

With the present geometric parameters of the chamber the BTI equations are fully covering the angular range up to $\psi_{\text{MAX}} = \pm 45^\circ$.

3.2 Hardware implementation of the BTI

The Bunch and Track Identifier was implemented in an ASIC, the best compromise between cost and performances. The chip was designed using the Standard Cell

technique in a CMOS 0.5 μ m technology with three layers of metal. The total area was 19mm² for 60k gates and prototypes were packaged either in a ceramic 68 pins LCC or in a 68 pins plastic TQFP. The BTI, when powered at 3.3V dissipates 200mW at 80MHz operating frequency. To get the best efficiency to noise ratio in the operating background conditions a careful setup is needed of programmable parameters like angular acceptance, time filters, drift velocity and wire dead time. The latency is equal to the maximum drift time (dependent on the programmed drift velocity) plus 100ns (8 clock cycles) for chip calculations. BTIs can be programmed either via a JTAG (IEEE Std 1149.1-1990) port or via a parallel interface using the trigger data bus for back-propagating parameters from the higher level devices [2]. System testability and visibility are good owing to built-in self test logic, snap registers insertion and boundary scan implementation. A block scheme of the BTI chip is shown in Figure 3.

The *Input Shapers* block is the interface to the 9 discriminated wire signals coming from the analog front-ends. An input latch is triggered by the rising edge of the signal, accepting a minimum pulse width of 3ns. Outputs are stretched to a programmable duration; during this time the input shaper is not retriggerable in order to reject high frequency double pulses. This parameter must be set according to drift velocity to minimize tube dead time.

In the *Pattern Logic* blocks all track patterns are evaluated in parallel. For each wire couple the Equations Counters compute the angle and the position of the crossing track according to the reference system introduced in Figure 2.

In the *Pattern Comparator* block the parent bunch crossing is identified looking for a matching of the k-parameters computed by the six equation counters relative to the four crossed tubes. The output is the matching value K, the position X and the quality bit H/L. The use of a quality bit allows the next device in the trigger chain to distinguish between clean tracks (alignment of four hits, i.e. six coincident k-parameters) and potentially wrong triggers (three out of four aligned hits, i.e. at least three coincident k-parameters) where can be classified the most of *ghost triggers*.

If several track patterns give a trigger at the same time, only one is selected by the *Priority Logic*, preferring a high quality track and using a default encoded order in case of multiple triggers with the same quality.

The BTIs send their data to higher level devices that associate the track segments and performs noise rejection. Indeed each BTI of the chamber outer Superlayer is interfaced to three Track Correlators (TRACO). In order to reduce the probability to generate multiple triggers from a single track, an angular filter was included and programmed to send to each TRACO only those tracks that could be fully contained in it. The trigger strobe is split into three signals activated only if the track k-parameter is within the relative programmable window of each TRACO. The quality bit line and the k-parameter/position bus are common to the three TRACOs. The BTI trigger output bus consists of the three trigger strobes, the quality bit and the 6 bit data bus where k-parameter and position are multiplexed at the clock speed.

In order to reduce the number of *ghost triggers*, the cancellation of LTRGs in the range (-1bunch crossing,+8bunch crossings) around a high quality trigger (Low Trigger Suppression) is a very efficient solution. The LTS logic block is latency inexpensive because it was inserted in the *Output Filter* pipeline, in parallel with the window comparator logic.

The *Control Logic* block contains a JTAG interface and a bidirectional parallel interface. The JTAG port can be used either to check chip interconnections during the PCB verification or to program internal registers. A built-in feature of this interface is the capability to monitoring chip activity without interference with the trigger function.

This can be performed accessing (using a SAMPLE instruction) the snap registers connected to the input signals and to the output bus.

The parallel interface, much faster than the JTAG one, can access all the BTI internal registers and is thought to be a backup solution for BTI setup. Using the trigger bus the downstream devices have the possibility to access the internal registers of the connected BTIs.

The BTI includes built-in self test logic (BIST) and emulation capabilities for testing purposes. In spite of the large input domain, chip validation can be performed using a set of 64k vectors only, thanks to the BIST circuitry.

Trigger diagnostics is possible using the BTI emulation mode. First the timing data of events to be tested are downloaded in the involved BTIs; then chips are programmed in emulation mode. When the specific trigger command is issued, the event is emulated at full speed and the relative trigger data can be found stored in the snap registers or can be directly read out with the programmed latency at the chip output.

A complete software model of the device was developed and interfaced to the full simulation of the CMS detector. Results of the simulation and details on the devices following the BTI in the trigger chain can be found in [9].

4. Sample selection

The recorded drift times were used to reconstruct beam tracks using a linear least squared fit. Only hits with drift times below 400ns were considered. The space-time conversion was linear using an average drift velocity of 56 $\mu\text{m}/\text{ns}$ as evaluated from the drift time boxes and all three or four points tracks with a χ^2 fit probability better than 0.1% were selected.

The time difference between the event trigger and the BTI internal clock is computed using a TDC channel with a 50ns jitter. This difference defines the synchronization time of any event and can be used to select the events finding their phase with respect to the BTI clock. The performance of the BTI as a function of the synchronization time is shown in Figure 4 for the HTRG signals in the standard configuration and in the minimum acceptance configuration acting on the alignment tolerance. As expected the dependence of the fraction of HTRGs on the synchronization time is a periodic function.

This dependence is much more important for the minimal acceptance than for the standard acceptance, because of the stricter requirement on alignment of the hits.

Hence there is a tight relationship between the time slot assignment and the phase: the phase corresponding to a unique time slot is the *right phase*. Since the period of the function is 25 ns there is a *right phase* every 25ns. The *right phase* is defined as the center of the synchronization time distribution of a time slot. It is obvious to choose as the *right time slot* the central one of Figure 4.

In order to define a synchronization acceptance window to select the events, a verification of the performance of the BTI as a function of the synchronization time is required.

The BTI efficiency is defined as the probability per event to have a trigger in the *right time slot*. The acceptance window will define an efficiency plateau. The result of a scan on the standard tolerance data with different synchronization time acceptance windows is shown in Table 1.

Furthermore, restricting the analysis to a subsample of clean four points fitted tracks, the probability to obtain an HTRG as a function of the synchronization time was

evaluated. Indeed Figure 5 shows that the probability of missing an HTRG in the $\pm 4\text{ns}$ range around the distribution center introduces only a 1% systematic effect in the evaluation of the HTRG fraction.

Summarizing, the final sample satisfies the following criteria:

- 3 or 4 points fitted track choosing the best χ^2 track with $\text{Prob}(\chi^2) > 0.1\%$
- fitted position falling within acceptance of the installed BTIs
- synchronization time within $\pm 4\text{ns}$ from the central value of the central time slot

In addition a BTI trigger is counted only if it is falling in the *right time slot*. Triggers occurring in the other slots are due to false alignments and are considered in the paragraph dedicated to noise evaluation.

5. Track Parameter resolution

5.1 Position studies

The BTI provides a position measurement in a reference frame with the origin on its left side (see Figure 2).

The BTI position can be converted into an absolute position: Figure 6 shows the correlation between the BTI computed position and the fitted track position for triggers issued in the *right time slot* only.

The difference between the computed position and the fitted position is given in Figure 7: the width of the distribution provides the BTI position resolution.

According to the used BTI configuration, the internal calculations are done using a 0.7mm least count and the trigger is output with a 1.4mm least count. The distribution should therefore have a width $\sigma \sim 1.4/\sqrt{12} \sim 0.4\text{mm}$ in the hypothetical case that all the events would fall in one bin.

The found resolution exhibits a slightly larger width, but it well agrees with expectations: HTRGs should have a better resolution than LTRGs, because of the larger lever arm for the calculation.

5.2 Direction studies

The performance check of the BTI angular calculations was done using cosmic rays. The BTI is not computing directly the track direction, but it determines a k-parameter related to the angle of incidence. The correlation between the measured k-parameter and the fitted track direction is shown in Figure 8. Although the angle itself is never internally used, for sake of clarity it is better to compare the measured and fitted angle, converting the computed k-parameter into the angle ψ . Their difference is shown in Figure 9, for different trigger qualities.

Once again the result matches expectations ($\sigma \sim 60/\sqrt{12} \sim 17\text{mrad} \sim 1\text{ degree}$).

6. Efficiency studies

Results were reported for the efficiency as a function of the synchronization acceptance window. Another interesting check is the efficiency in the different configurations that were used for the BTI. The results for normal incident muons are summarized in Table 2. The relative fraction of LTRGs and HTRGs is consistent with

the already measured probability of δ -ray generation in the interaction of the muon with matter[4].

It is clear that the BTI inefficiency is negligible, but it is also evident that the LTS mechanism, activated for all configurations except the first one, is cutting a small amount of good triggers.

Summing the HTRG fraction to the LTRG one, the overall trigger rate is roughly constant in all cases. Therefore in the minimal acceptance configuration there is just a different population, with HTRGs becoming LTRGs, rather than the creation of inefficiencies.

The maximal acceptance configuration result shows that the acceptance requirement provided by the standard configuration is sensible, since no real efficiency gain is obtained relaxing the alignment tolerance.

The uniformity of the BTI response along the cell is shown in Figure 10: the BTI efficiency as a function of the particle impact point at normal incidence is flat. This fact implies that the drift cells design has indeed met the basic linearity requirements.

But the space-time linearity relation required to assure a correct performance of the BTI is not achievable in the whole angular range. The BTI is still able to trigger correctly until the deviation from linearity is below 25ns, but at very large angle there are much bigger deviations.

Figures 10 and 11 show respectively the behaviour of the BTI trigger efficiency and the probability of out of time triggers in selected angular intervals, separately for the full sample and the four hits sample.

The BTI response is almost flat up to about an angle of incidence of 30° . Beyond this value the BTI starts to fail in finding alignments of four hits at the *right time* and simultaneously the probability of finding an out of time HTRG increases. The failure is dramatic for the full sample and rather more limited for the sample of fitted four hits tracks. This fact confirms that the HTRG loss is not due to errors in the BTI design but to the unavoidable linearity degradation of the cell with increasing incidence angle.

The out of time triggers are mostly issued in the time slot just before *the right time slot*. Therefore activating the LTS mechanism a fraction of the good LTRGs will be canceled. Unfortunately LTRGs will be dominant at very large angle. Anyway it is important to remind that the chamber was the first full size prototype and improvements in its performance should be expected in the final version.

7. Noise studies

There are two possible causes for multiple BTI triggers:

- redundancies, i.e. angular range superposition between different equations, causing a trigger on the adjacent BTI at the same time slot as the real trigger
- temporal ghosts due to random alignments on the same BTI at time slots other than the one corresponding to the real trigger.

Figure 12 gives the distribution of the average number of HTRGs and LTRGs per event, showing that there are sometimes two HTRGs and that a muon is generating a large quantity of LTRGs.

We will try to understand in detail the ghost population at normal incidence with the test beam data.

7.1 Redundancy noise

In order to understand the redundancy noise we have to limit the muon track position to the acceptance of one BTI only. We chose as reference BTI the sixth one, because of the higher statistics available. The first half of BTI # 6 is superposed to the second half of BTI # 5. Therefore the redundancies will give in some case a trigger in both BTIs. Asking for a track inside BTI # 6 acceptance, we can find the probability of another trigger (HTRG or LTRG) to be generated in the nearby one. The data are collected in Table 3.

The probability of a redundant LTRG is very high, but a filter in the devices following the BTI in the trigger chain is provided to reject this trigger topology [9]. Therefore only cases where two triggers of the same quality are associated are relevant.

The most critical situation arises when the two triggers are both HTRGs, because the selection logic will always send twice the same track.

The spatial distribution of double HTRGs is shown in Figure 13.

The tracks are concentrated in the border region between two BTIs. This fact leads to identify pattern 5L7L6R8L that is partially superposed with pattern 1R3L2R4L and if a track is close to the wire both patterns trigger. Since patterns can be individually disabled, it is possible to fix this particular problem without revising the BTI design.

7.2 Temporal ghosts

The BTI trigger algorithm can actually work requiring only three layers of staggered tubes. The drawback of this kind of choice is the fact that an inefficiency or a bad measurement on any of the cells becomes an inefficiency or a wrong trigger. The introduction of the fourth layer with the minimal request of an alignment of three out of four hits enhances the efficiency and reduces the wrong measurements. But some spurious alignments of three hits can occur at any bunch crossing, depending on the track position and direction.

Most of the bad alignments are generated from the unavoidable left-right ambiguity even at several bunch crossings distance from the alignment of the four hits.

An example of the mechanism is shown in Figure 14, where a real track orthogonal to the chamber is displayed and the hit positions are marked with small circles on the track line. The BTI, looking for alignments of at least three hits, is able to find the alignment corresponding to the real track, but two other tracks are detected. These tracks, called *ghost tracks*, correspond to alignments of a mixture of real hits and their mirror images. Infact the BTI supposing that wire 2 is inefficient and that the signal of wire 4 comes from the right side of the tube, finds a false alignment at time Δt_1 after the right bunch crossing. In the same way, supposing that wire 5 is inefficient, the BTI finds another *ghost track*, formed from the signals of wires 2 and 4 and the mirror image of signal from wire 3, at time Δt_2 before the right bunch crossing.

Figure 15 shows the time distribution of BTI # 6 triggers for HTRGs and LTRGs in the standard configuration and for LTRGs, once the Low Trigger Suppression is activated.

There is a low probability to issue an HTRG at the wrong time slot, while there is a large number of wrong LTRGs. The average fraction of wrong triggers per event in the different configurations is given in Table 4. The noise reduction caused by the LTS mechanism is evident.

Some of the wrong HTRGs are due to noise hits: one of the drift times is different than expected and the alignment occurs around the right angle and position, but at a wrong time, and only a LTRG is issued at the right time. This effect is causing a small efficiency drop when the LTS mechanism is activated, since the right LTRG is cancelled by the nearby wrong HTRG.

But there is a special category: about 2% of the times there are two HTRGs on the same BTI at different time slots relative to the same event. The crossing position of the tracks generating this kind of triggers is shown in Figure 17: it is clear that most of the triggers are generated from tracks traversing the cell in a special position. Furthermore the angular parameter of the ghost trigger is always the same ($\sim 55^\circ$). This is one well-known HTRG ghost track. While it is easy to get rid of this false trigger just limiting the output range to $\pm 45^\circ$, the existence of this ghost track causes an equivalent rate of failures of the LTS mechanism, due to its non-retriggerable nature.

8. Radiation Tests

The data were taken in the CERN GIF test area where a 15 Ci ^{137}Cs radiating 66 MeV source is installed. It was therefore possible to test the performance of the trigger in a radiation environment. Data were taken using several filters in front of the source reaching a single hit rate of 10 Hz/cm^2 on the chamber: this rate is the maximum expected rate at LHC in the barrel muon detector due to neutron and gamma background.

The data were compared to those without radiation looking for differences in the efficiency, the noise probability and the position resolution.

Results for efficiency and noise are collected in Table 5.

The position resolution is reported in Figure 18. No significant effect is seen, but a large increase of out of time LTRGs and a slight deterioration of the LTRG position resolution. The noise filters provided in the trigger chain are expected to cope easily with this background.

Therefore the BTI concept is well suited to work in the foreseen radiation environment.

9. Conclusions

The behaviour of the ASIC prototype version of the BTI was thoroughly investigated and the performance of the device is completely understood.

The results on efficiency and resolution confirm the validity of the design choices and are matching all the previously performed computations.

The implemented algorithm was found to be quite safe in a high radiation environment.

Acknowledgements

We thank the people working in the mechanical workshop in Padova who built the chamber under the supervision of Dr. Ing. C. Fanin and Dr. Ing. M. Benettoni.

The design of the electronics boards and their mounting was carefully done by L.Castellani, M. Cavicchi, R. Giantin and G. Pitacco.

We acknowledge the help of the people of the Muon Barrel group of CMS for the various activities done during test beam data taking.

References

- [1] CMS Technical Proposal, CERN LHCC 94-38, LHCC/P1 (1994)
- [2] M. De Giorgi et al, *Proceedings of the Fourth Workshop on Electronics for LHC experiments*, CERN LHCC 98-36 (1998) 285
- [3] G. Dallavalle et al, *Proceedings of the Fourth Workshop on Electronics for LHC experiments*, CERN LHCC 98-36 (1998) 294
- [4] M. Benettoni et al, Nucl. Instr. and Meth A.410 (1998) 133
- [5] F. Gonella and M. Pegoraro, *Proceedings of the Fourth Workshop on Electronics for LHC experiments*, CERN LHCC 98-36 (1998) 257
- [6] G. Dallavalle et al, *Proceedings of the Fourth Workshop on Electronics for LHC experiments*, CERN LHCC 98-36 (1998) 291
- [7] M. Passaseo et al., Nucl. Instr. and Meth A 367 (1995) 418
- [8] F. Gasparini et al, Nucl. Instr. and Meth A 336 (1993) 91
- [9] M. De Giorgi et al, *Proceedings of the First Workshop on Electronics for LHC experiments*, CERN LHCC 95-96 (1995) 222

Figure Captions

- Fig. 1 - Layout of the drift cell.
- Fig. 2 - BTI geometric layout showing the channels allocation and important parameters.
- Fig. 3 - BTI block scheme.
- Fig. 4 - High Quality trigger time slot assignment as a function of the synchronization time.
- Fig. 5 - Probability of missing an HTRG in a clean four hits tracks sample as a function of the synchronization time.
- Fig. 6 - Correlation between BTI position parameter and track fitted position. All triggers in the *right time slot* were included.
- Fig. 7 - Position resolution for different trigger qualities.
- Fig. 8 - Correlation between the computed k-parameter and the fitted angle. All triggers in the *right time slot* were included.
- Fig. 9 - Angular resolution for different trigger qualities.
- Fig. 10 - Efficiency of the BTI at normal incidence as a function of the crossing point inside the drift cell.
- Fig. 11 - Relative fraction of HTRGs (full symbols) and LTRGs (open symbols) in the BTI as a function of the muon angle of incidence. The circles refer to the subsample of fitted four points tracks, while the squares refer to the full selected sample. The efficiency of the BTI is given by the sum of HTRGs and LTRGs and is 100% everywhere except at normal incidence due to the presence of the walls of the drift tubes.
- Fig. 12 - Probability per event of double HTRGs in the same BTI at different time slots as a function of the muon angle of incidence.
- Fig. 13 - Number of triggers per event for different trigger qualities.
- Fig. 14 - Position of the tracks giving double HTRG triggers in different BTIs at the same time slot
- Fig. 15 - Sketch of the generation mechanism of *ghost tracks* inside the BTI.
- Fig. 16 - Time distribution of BTI output triggers, for different trigger qualities and configurations.
- Fig. 17 - Fitted position of tracks generating double HTRGs on the same BTI at different time slots. The track fitted position is measured in the BTI reference frame: i.e. the wire/wing positions of the cells are every 2cm, starting at $x=0$.
- Fig. 18 - BTI position resolution in a radiation environment of 10 Hz/cm^2 single hit rate.

Synchronization range	$\pm 2ns$	$\pm 4ns$	$\pm 6ns$	$\pm 8ns$	$\pm 10ns$	$\pm 12ns$
HTRG fraction	84.3%	83.0%	81.7%	79.0%	75.0%	70.5%
LTRG fraction	14.5%	15.4%	16.7%	19.4%	23.3%	27.8%
Efficiency	98.8%	98.5%	98.5%	98.5%	98.3%	98.3%

Table 1 – BTI performance for different synchronization time acceptance windows.

BTI acceptance	LTS	HTRG fraction	LTRG fraction	Inefficiency
Standard	off	84.0%	15.6%	0.3%
Standard	on	85.1%	13.6%	1.3%
Minimum	on	70.7%	28.2%	1.1%
Maximum	on	84.8%	13.8%	1.4%

Table 2 – Efficiency figures for the tested configurations.

HTRG only on BTI 6	5.1%
HTRG on BTI 6 and HTRG on BTI 5	4.4%
HTRG on BTI 6 and LTRG on BTI 5	74.0%
LTRG only on BTI 6	10.1%
LTRG on BTI 6 and HTRG on BTI 5	0.4%
LTRG on BTI 6 and LTRG on BTI 5	5.9%

Table 3 – Probability of a redundancy trigger in adjacent BTIs at normal incidence.

BTI acceptance	LTS	%H out of time	%L out of time
Standard	off	3.0%	351.2%
Standard	on	3.1%	148.2%
Minimum	on	1.1%	175.6%
Maximum	on	4.1%	165.3%

Table 4 – Average fraction of out of time triggers at normal incidence.

	%HTRG	%LTRG	Inefficiency	%H out of time	%L out of time
No Radiation	84.0%	15.6%	0.3%	3.0%	351.2%
Radiation 10 Hz/cm ²	83.0%	16.6%	0.5%	2.5%	800.0%

Table 5 – Comparison at normal incidence between performance without radiation and maximum radiation.

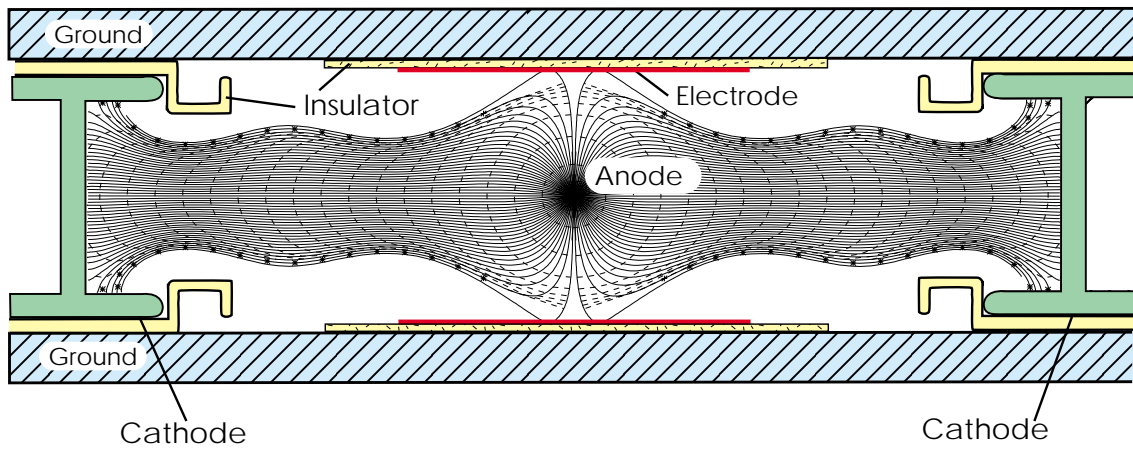


Figure 1

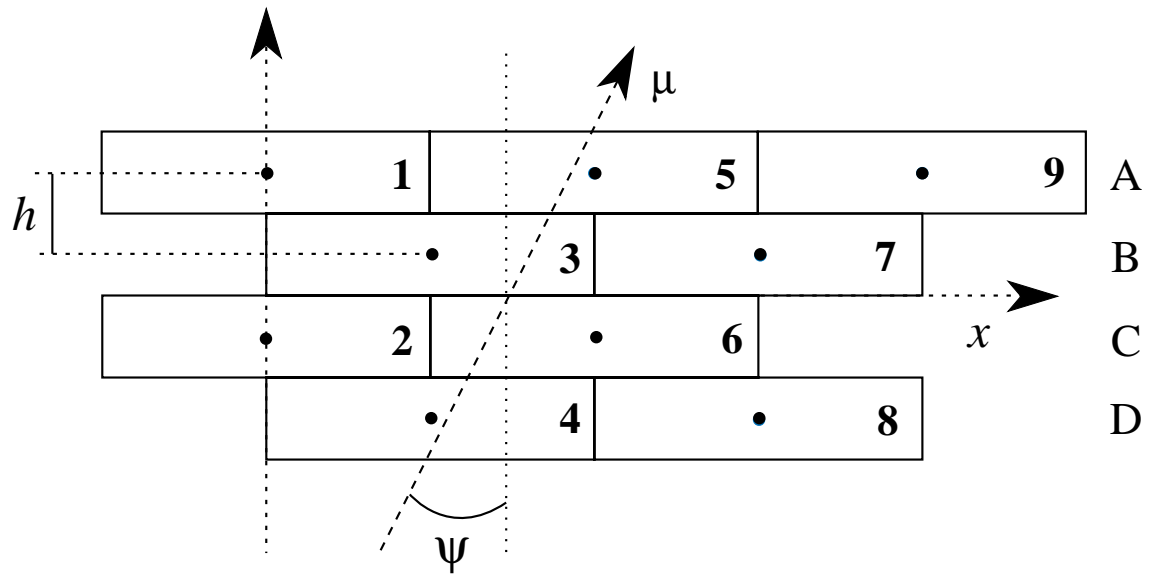


Figure 2

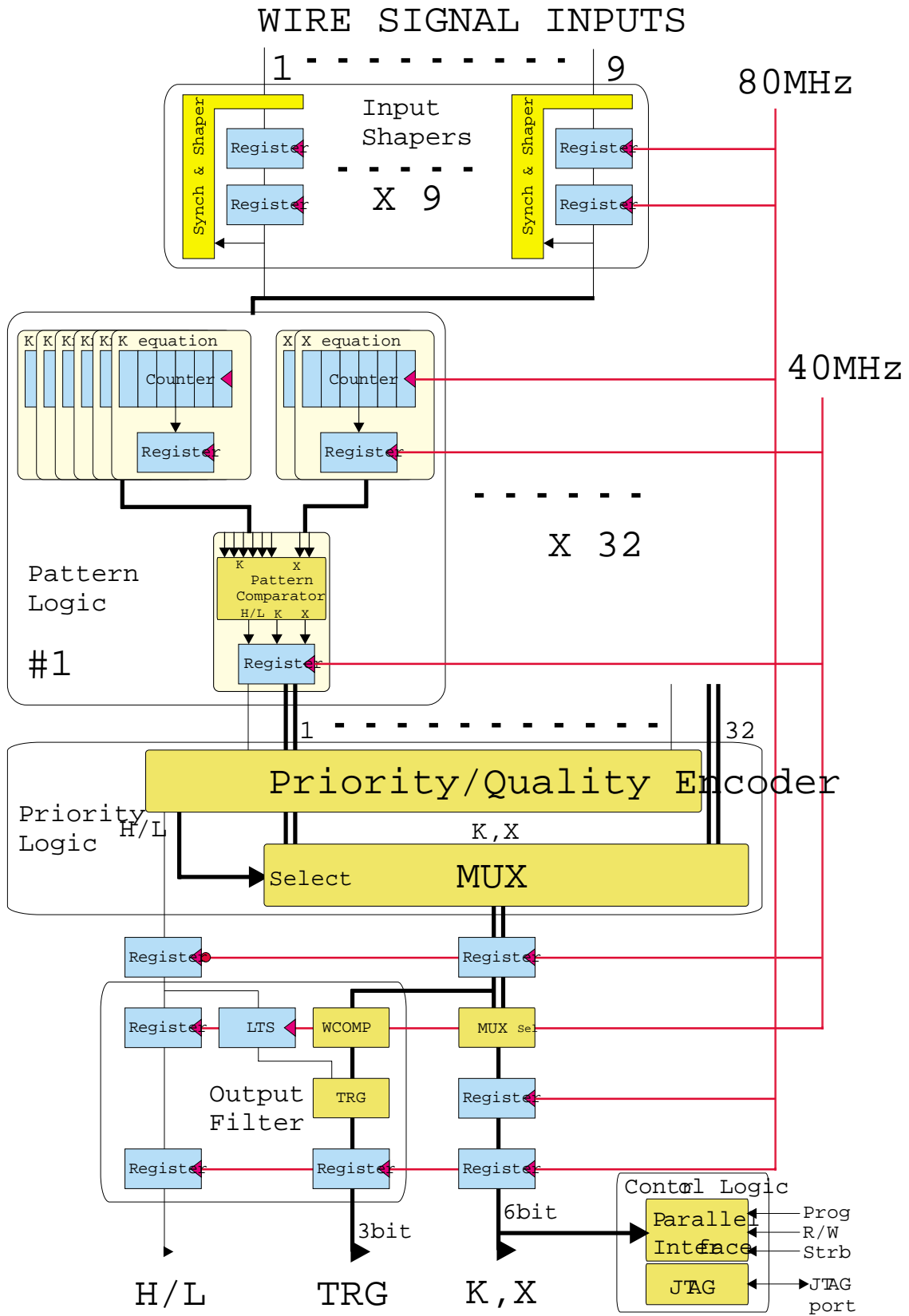


Figure 3

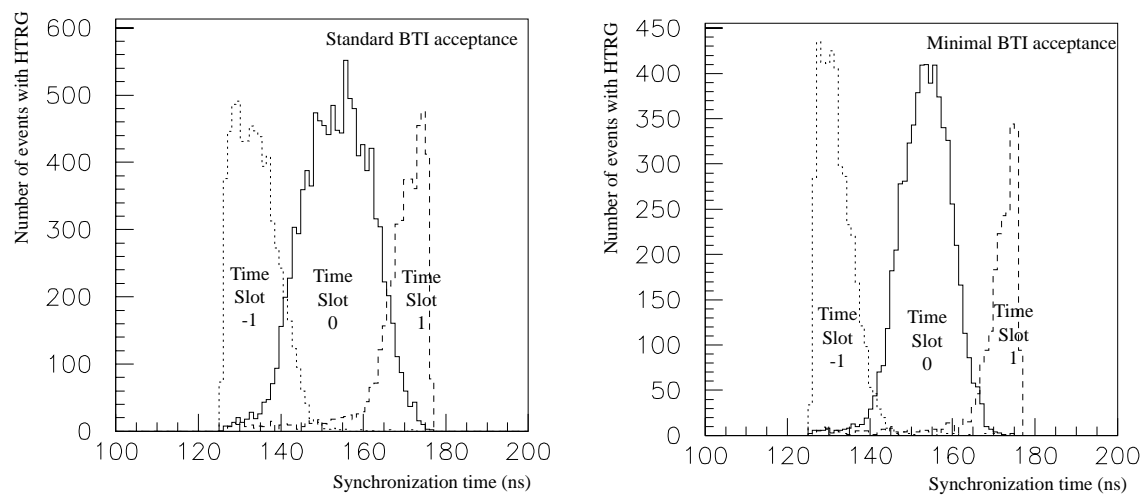


Figure 4

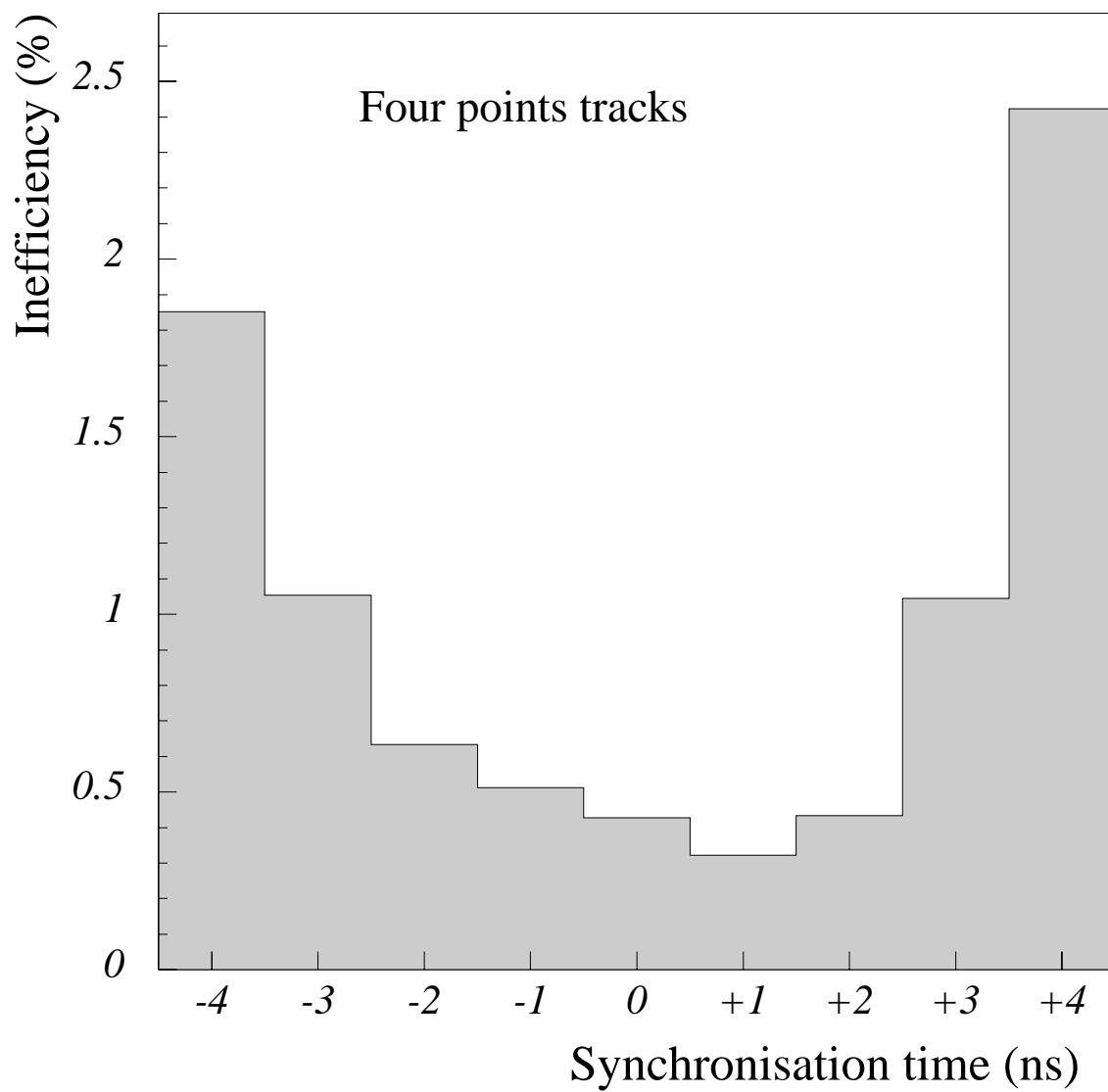


Figure 5

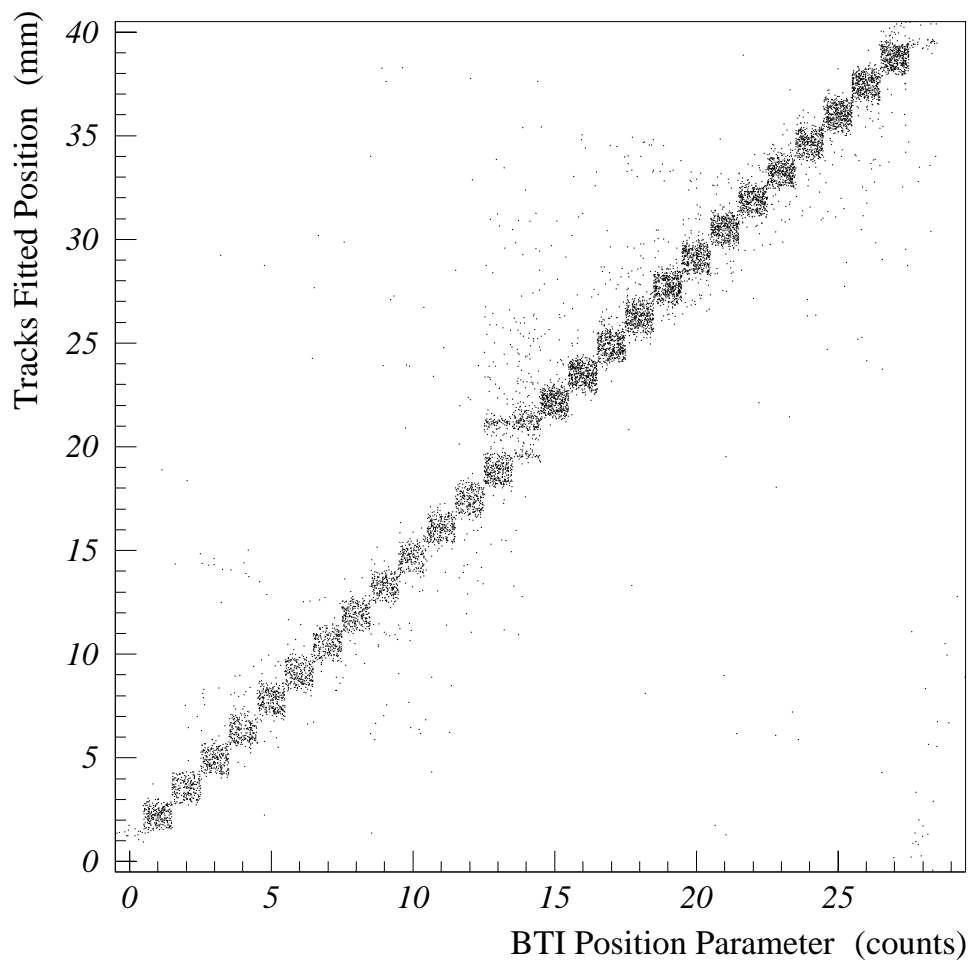


Figure 6

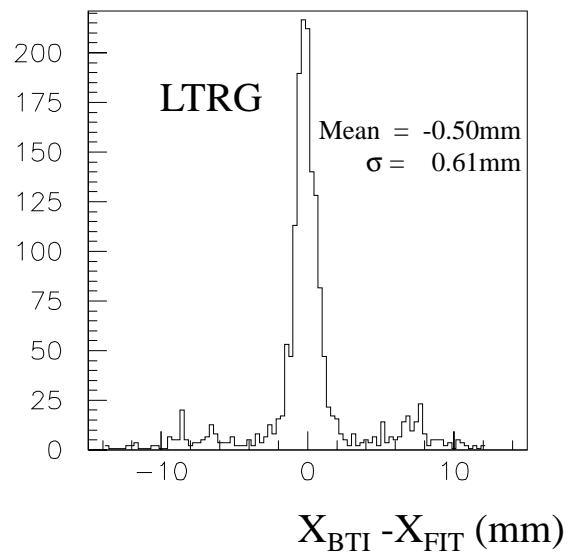
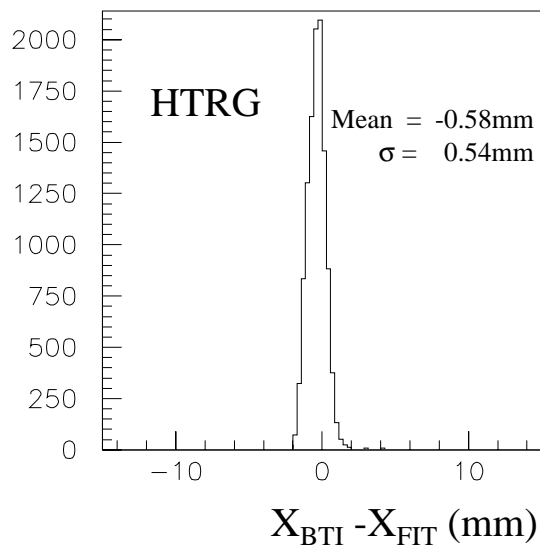


Figure 7

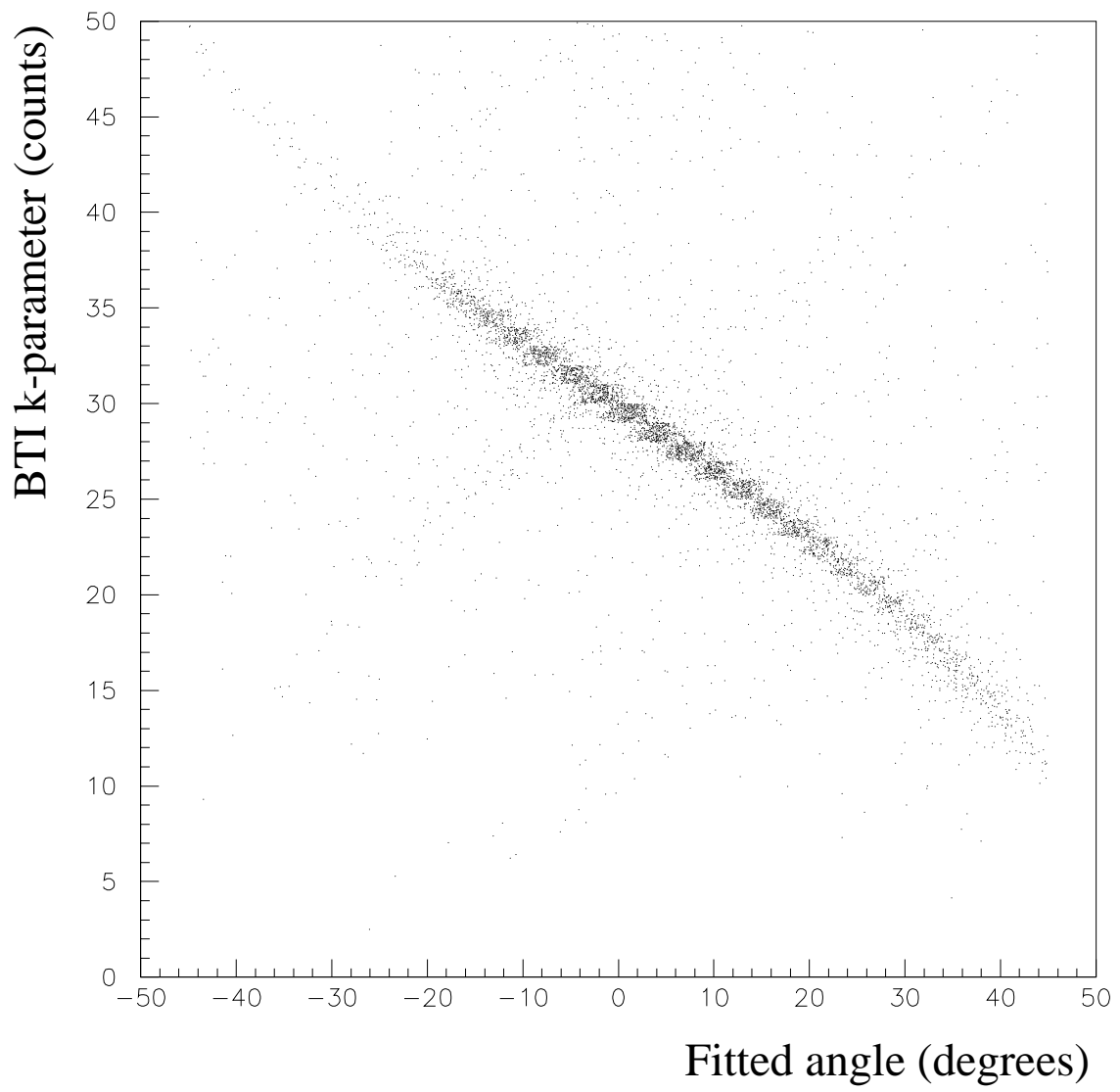


Figure 8

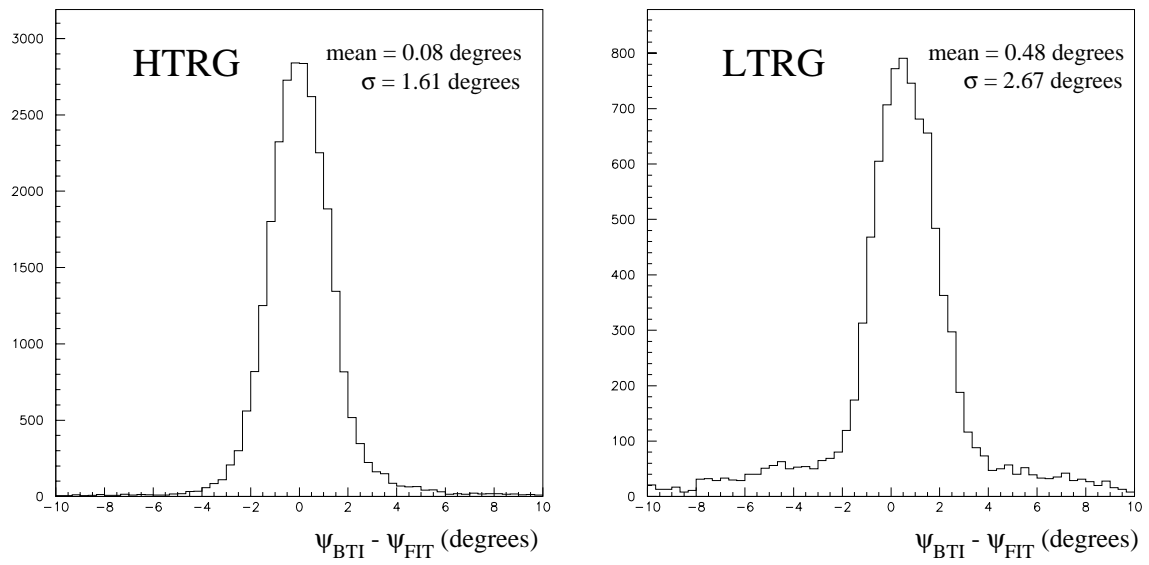


Figure 9

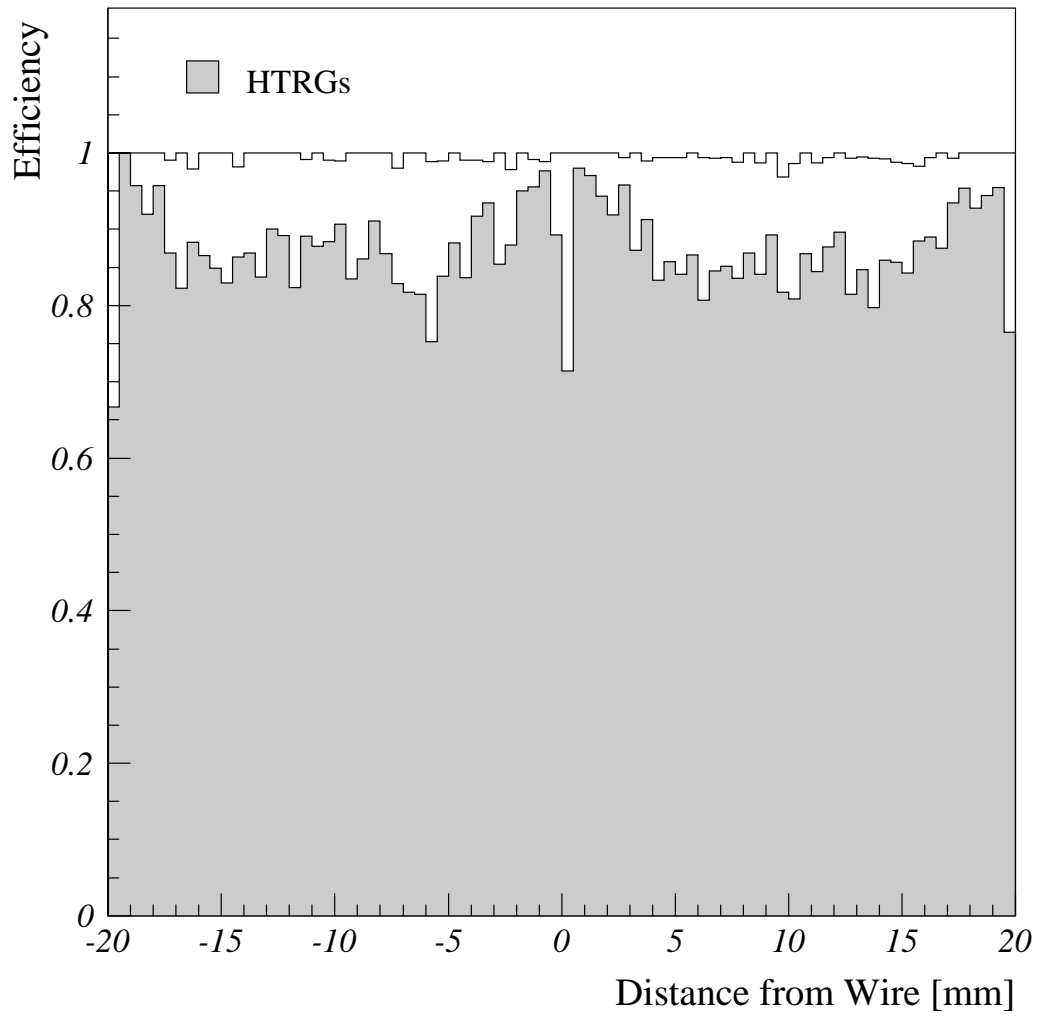


Figure 10

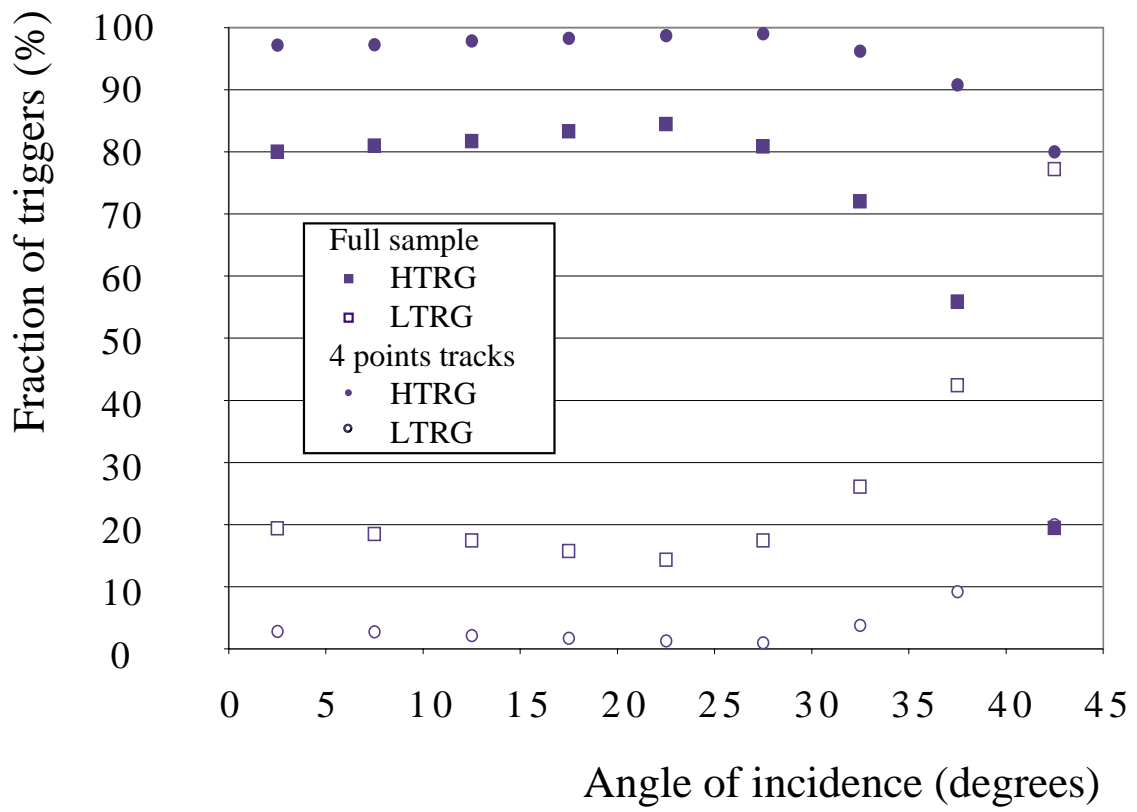


Figure 11

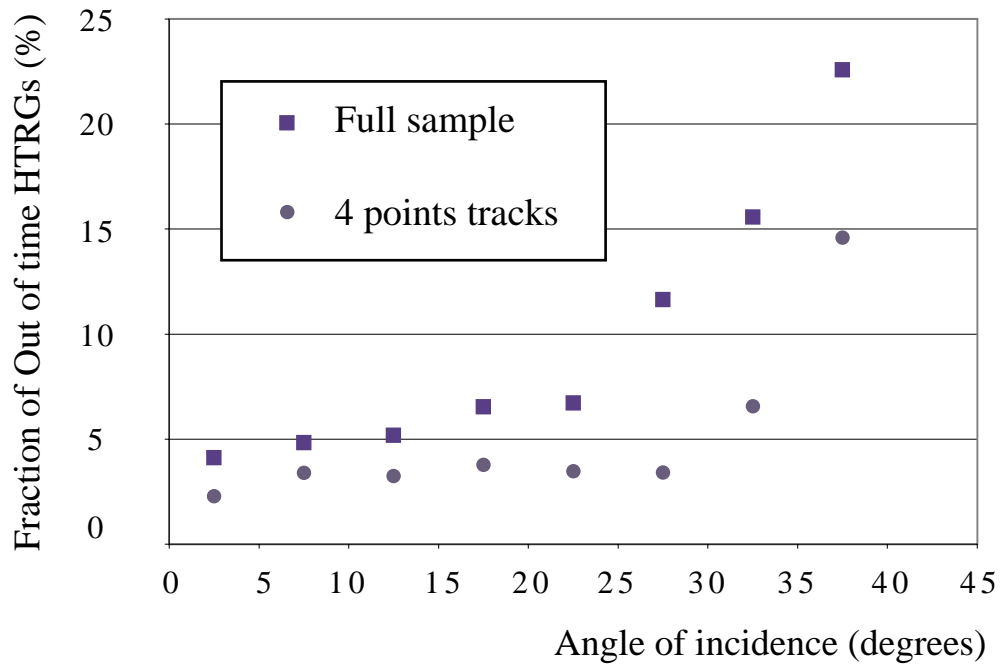
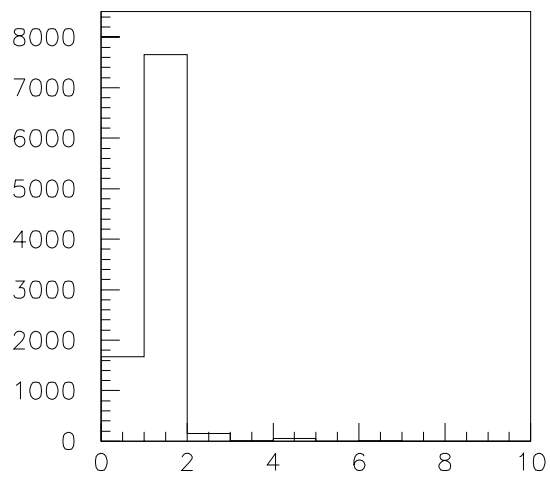
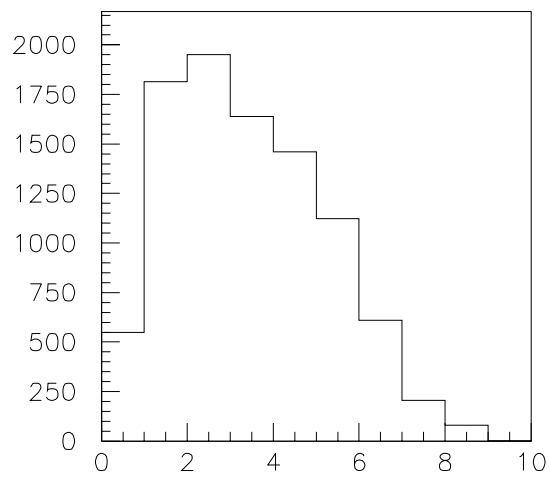


Figure 12



Number of HTRGs per event



Number of LTRGs per event

Figure 13

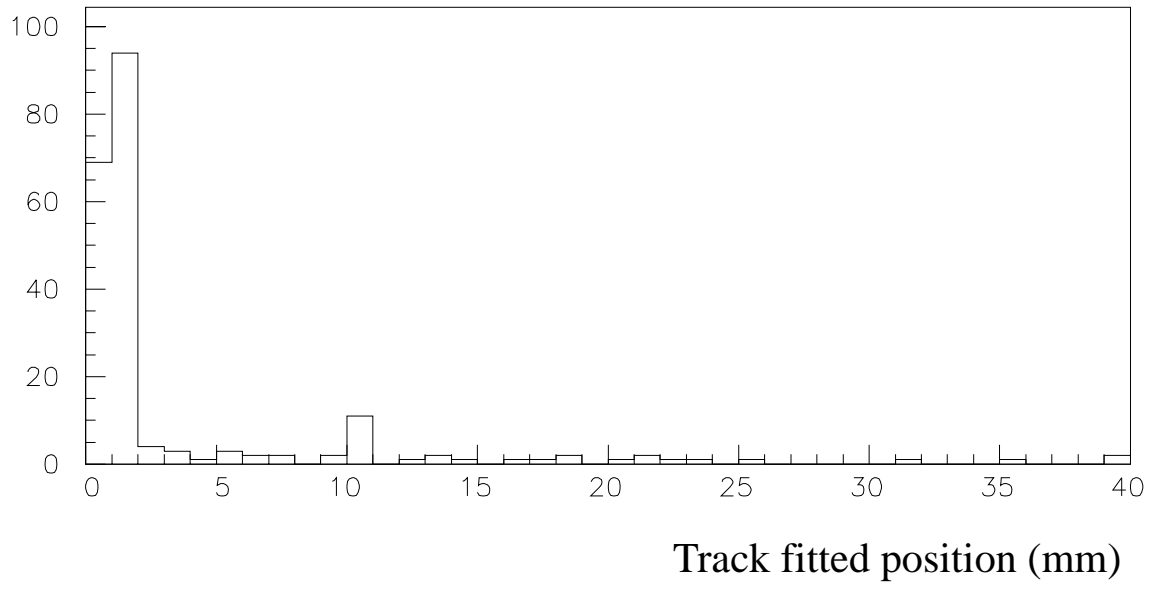


Figure 14

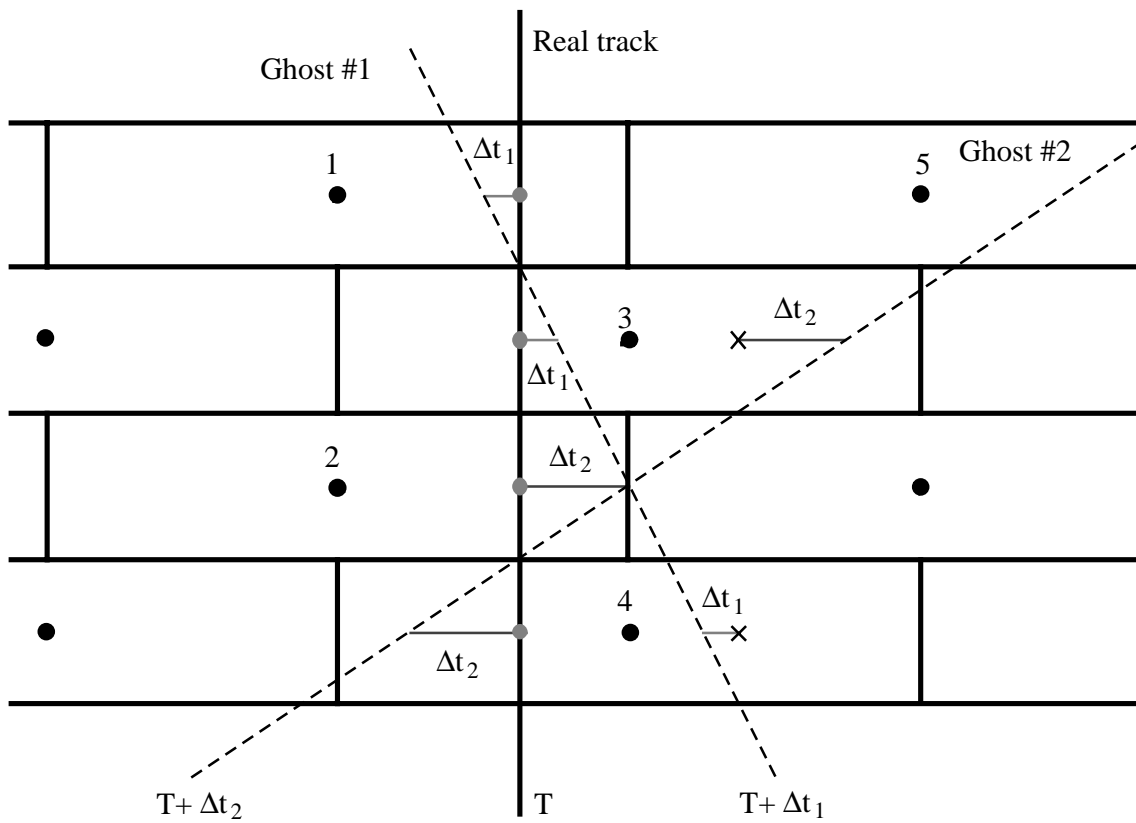


Figure 15

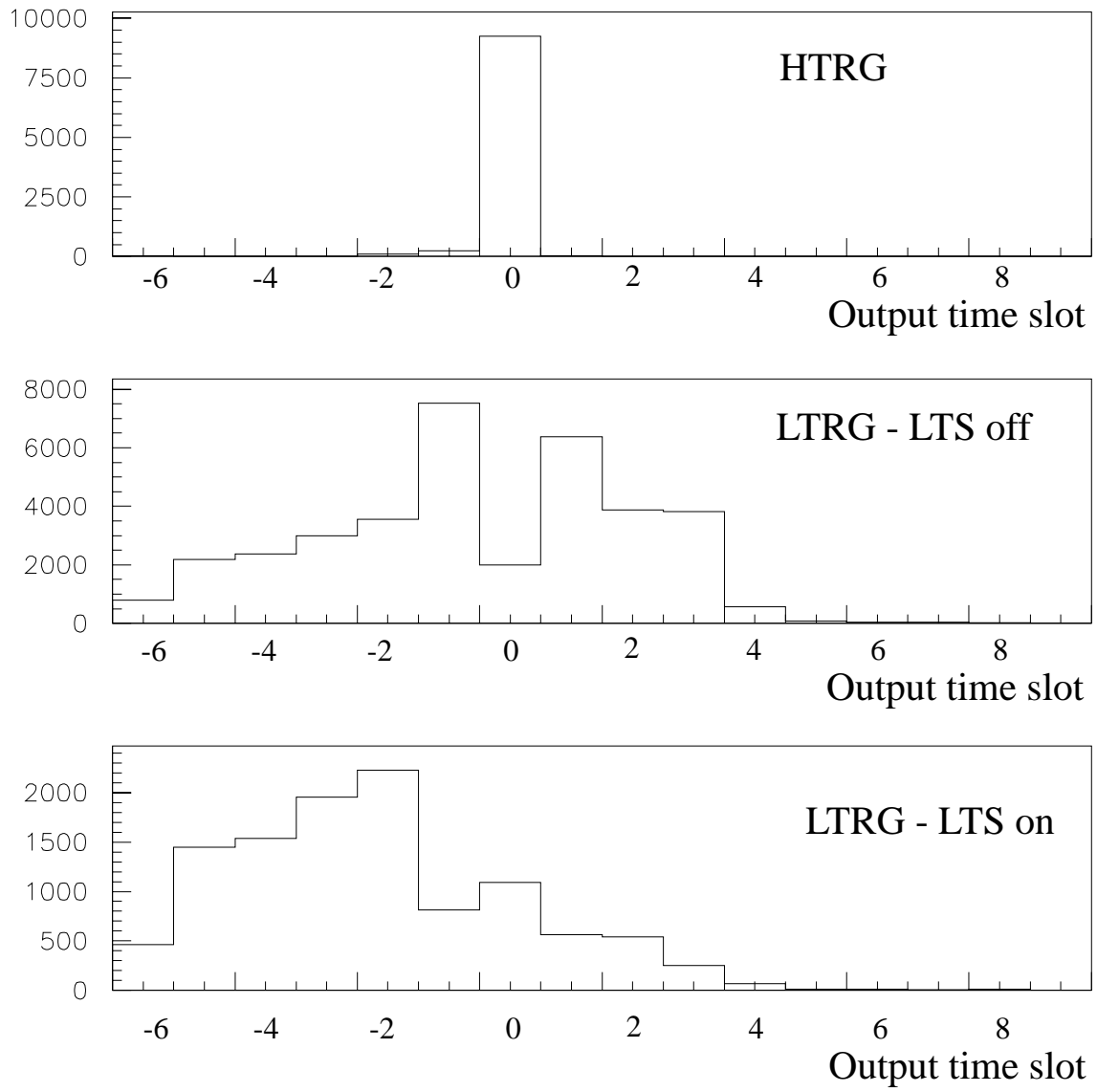


Figure 16

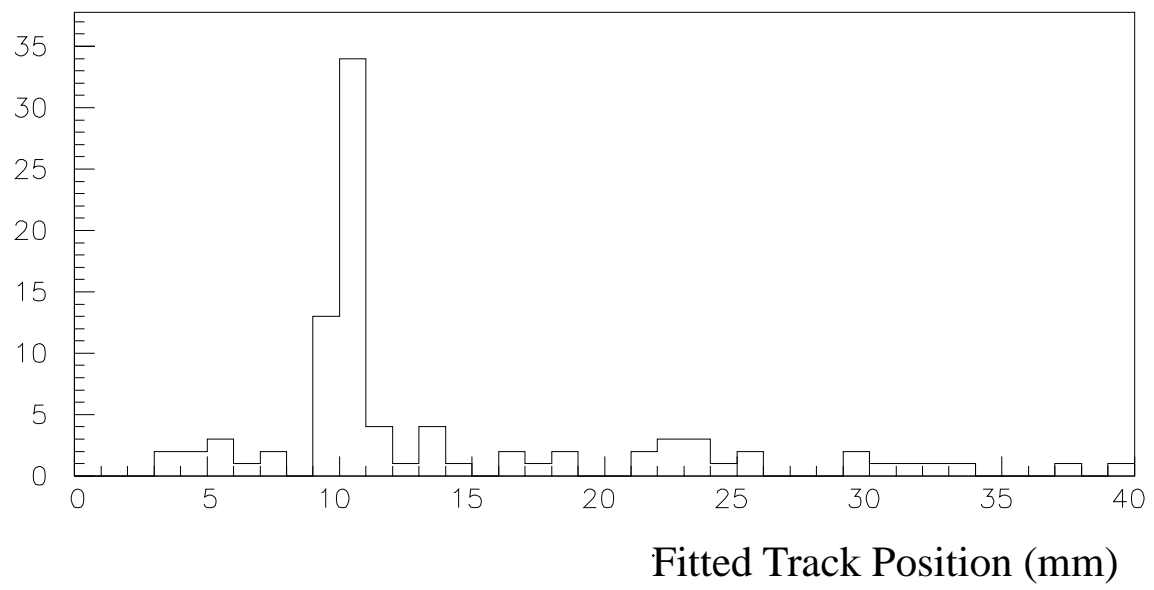


Figure 17

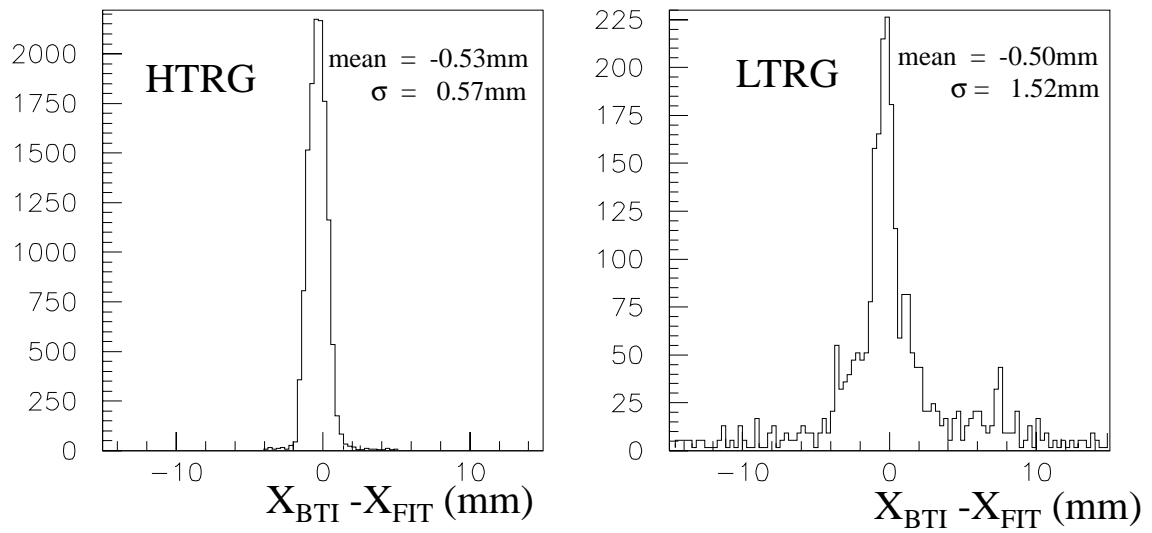


Figure 18